Nanoscale

Accepted Manuscript

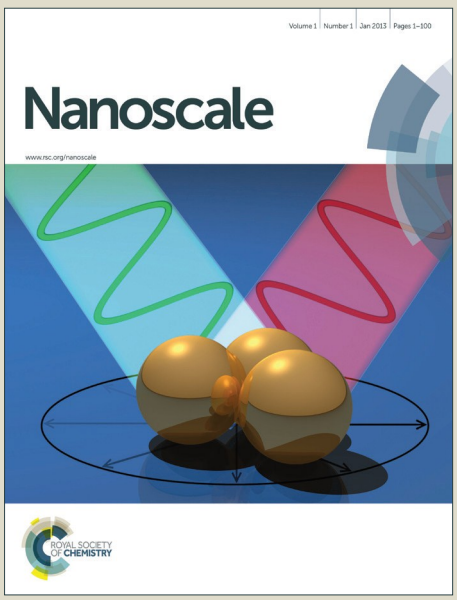

ROYAL SOCIETY OF CHEMISTRY

www.rsc.org/nanoscale

Nanoscale

Article

One-step detection of pathogens and cancer biomarkers by naked eyes based on aggregation of immunomagnetic beads

Received 00th January 20xx,
Accepted 00th January 20xx

DOI: 10.1039/x0xx00000x

www.rsc.org/

Yiping Chen,[a※] Yunlei Xianyu,[a※] Jiashu Sun,[a] Yajing Niu,[a] Yu Wang,[b] and Xingyu Jiang[a]*

This report shows that immunomagnetic beads (IMBs) can act as the optical readout for assays, in addition to serving as the carrier for purification/separation. Under the influence of an external magnetic, IMBs are attracted to coat one side of a test tube. IMBs specifically bound to targets can form a narrow brown stripe, whereas free IMBs will form a diffuse, yellow coating on the side of the test tube. Target analytes can aggregate initially dispersed IMBs in a sample concentration-dependent manner, yielding a color change from yellow to brown that can be read with the naked eye. This assay combines the convenience of lateral flow assays that allows one-step assay to finish within 15 min, and the sensitivity of enzyme-linked immonosorbent assay.

Introduction

Sensitive, rapid and low-cost detection of biomacromolecules and pathogenic microbes is becoming important for food safety, environmental monitoring and clinical diagnosis.[1-3] Currently, detections of biomacromolecules and microbes are generally based on one or several of the following types of assays: polymerase chain reaction (PCR),[4] enzyme-linked immunosorbent assay (ELISA),[5, 6] and gold lateral flow strip (GLFS).[7] PCR has a high sensitivity, however, it requires complex manipulation and expensive instruments. ELISA has been widely used in detecting biomacromolecules because of its specificity, sensitivity and low cost. Nevertheless, as a heterogeneous assay, ELISA is labor-intensive and time-consuming because of its washing steps. GLFS is simple, rapid and low-cost, but its sensitivity is lower than other methods. Although the requirement of point-of-care (POC) detection has promoted the development of technologies that have largely improved conventional methods,[8-10] there is still of a great need to develop a simple, sensitive, low cost and rapid approach for POC testing.[11, 12]

Recently, sensors that based on the aggregation of gold nanoparticles (AuNPs) have drawn increasing attention due to their high sensitivity and straightforward readout.[13-15] However, AuNPs-based sensors need complex purification/separation procedures that may limit their large-scale applications in the POC testing. Immunomagnetic beads (IMBs) have attracted considerable interest in the field of biosensors and bio-separation due to their excellent optical and magnetic properties.[8, 16-18] Many researchers have developed ultrasensitive methods for detection of biomarker using a signal amplification system based on super-paramagnetic particles.[19-21] For example, an assay for quantification of DNA in biological samples via aggregation of super paramagnetic bead shows that IMBs can aggregate and show visible change of patterns.[22] We find that the state of aggregated multiple-IMBs in magnetic field differs from that of dispersed IMBs in immuno reactions, and the degree of aggregation of IMBs is related to the concentration of target. We further hypothesize that IMBs not only can be used as magnetic separation carrier, but also can act as a visual signal in immuno reactions. If we integrate the magnetic separation and readout procedure, the operation can be simplified and the assay time will be shortened. The target (pathogenic bacterium or protein) can selectively bind the dispersed IMBs by specific antibody-antigen interaction, thus can aggregate IMBs in the presence of magnetic fields. The aggregated IMBs will present a brown color with a narrow stripe, distinguished from dispersed IMBs (a diffuse, yellow coating). Furthermore, the degree of aggregation of IMBs is sample concentration-dependent, thus allowing the possibility of quantification. Compared to AuNPs sensors that enable the naked-eye readout, this IMBs-based sensor not only allows an optical readout for assays, but also serves as the carrier for

[a] *Beijing Engineering Research Center for BioNanotechnology and CAS Key Laboratory for Biological Effects of Nanomaterials and Nanosafety, National Center for NanoScience and Technology, Beijing 100190, China; E-mail: xingyujiang@nanoctr.cn.*
[b] *Address here. Beijing Institute for Tropical Medicine; Beijing Friendship Hospital, Capital Medical University, 95,Yongan Road, Xicheng District, Beijing, 100050, China*
※ *These authors equally contribute to this work*

† Footnotes relating to the title and/or authors should appear here.
Electronic Supplementary Information (ESI) available: [details of any supplementary information available should be included here]. See DOI: 10.1039/x0xx00000x

purification/separation that greatly simplifies the assaying procedures.

In this study, we develop a visual immunosensor for one-step detection of bacteria and cancer biomarkers *via* the aggregation of IMBs. IMBs are not only used as the magnetic separation carrier to capture and enrich the target from samples, but also used as a visual signal to indicate the amount of target analytes in samples (Figure 1). To our knowledge, it is the first report that the immunomagnetic aggregation (IMA) sensor combines the magnetic separation and visual readout in one step for the detection of biomarkers.

Experimental

Reagents and Materials

Magnetic beads (MBs) (1000, 500, 200 and 130 nm in size, solid content: 10 mg/mL) were purchased from Estapor Super paramagnetic Microspheres (Millipore, USA). *Escherichiacoli* (*E. coli*), *Salmonella spp (S. spp), Shigella spp, Staphylococcus aureus (S. aureus)* and *spirillum cholera* (*S. cholera*) were obtained from the American type cells collection. *Anti-E. coli* polyclonal antibody (ab25823) was purchased from Abcam (USA). Alpha fetal protein (AFP), carcino-embryonic antigen (CEA), a pair of monoclonal antibodies that recognize the AFP (6.4 mg/mL and 3.2 ng/mL) and a pair of monoclonal antibodies that recognize the CEA (4.9 ng/mL and 5.4 ng/mL) were purchased from Beijing Hotgen biological technology (Beijing, China). 1-ethyl-3-(3-dimethylaminopropyl)-carbodiimide hydrochloride (EDC), bovine serum albumin (BSA), and N-hydroxysulfosuccinimide sodium (Sulfo-NHS) were purchased from Sigma-Aldrich (USA). Other reagents and solvents were of analytical grade and were purchased from Beijing Chemical Reagents Co. (Beijing, China). The water used in the experiments was deionized and ultrafiltered using a Milli-Q apparatus.

Apparatus

The magnetic separation rack (0.05T) was from Shanghai Allrun Nano Science and Technology Co., Ltd (Shanghai, China). MS3 vortex oscillator (IKA Inc, Germany) was employed to mix samples and IMBs solution.

E. coli culture

The pure culture of *E. coli* was grown in luria broth (LB, tryptone 1%, sodium chloride 1%, yeast extract 0.5%) on an orbital shaker at 37 ^{o}C for 20 h before use. *E. coli* number was determined by conventional plate counting 0.01 mL of *E. coli* dilutions. *E. coli* colonies on the plate were counted to determine the number of colony-forming units per milliliter (cfu/mL).

Preparation of IMBs

2 mg of magnetic beads was suspended in 2 mL of activated buffer (80 nM MES, pH=5.2). Then, 80 μL of EDC (10 mg mL^{-1}) and 40 μL of NHS (10 mg mL^{-1}) were added to the MBs solution. After activation for about 30 min, the excess EDC, NHS and byproducts were removed *via* magnetic separation using a magnetic scaffold. Then 2 mL of PBS buffer (pH=7.4, 0.01M) was added to re-suspend the activated MBs. Subsequently, 0.1 mg Ab (anti-*E. coli* antibody, anti-CEA antibodies or anti-AFP antibodies) was added to the activated MBs solution. The mixture was gently stirred to react for 2 h at room temperature and then blocked with 1% (m/v) BSA for 0.5 h. The IMBs were separated from the free $Ab_{1,}$ re-suspended in 1000 μL of PBS and stored at 4 ^{o}C for further use.

Procedure of IMA sensor

The procedure was illustrated in Scheme 1. First, 100 μL of IMBs solution and 900 μL of different concentrations of *E. coli* (10^7, 10^6, 10^5, 10^4, 10^3, and 0 cfu/mL) were transferred to centrifuge tubes (2 mL or 1.5 mL). Each mixture was gently shaken for 10 min. Then all the tubes were put on a magnetic scaffold, and the state of IMBs can be observed after 1 min. The pictures of the state of IMBs were recorded by a digital camera, and the color of IMBs is transferred into gray-scale values by the Ellipsometric Imaging Expert System (EIES).The gray-scale value directly reflects the brightness of color of IMBs, which is related to the degree of aggregation of IMBs. We use software Origin 8.0 for the statistical analysis.

Real sample analysis

Water samples were collected from a local river (Tonghui River, Beijing) and a livestock farm (Chaoyang District Farm) in Beijing. The samples were centrifuged at 1000 r/min for 5 min, and the supernatant was collected for analysis. Urine samples were collected from healthy people in our laboratory. The clinical serum samples (positive samples and negative samples) were collected from Tiantan hospital (Beijing, China) and the samples were 100-folds diluted for analysis.

Results and discussion

The principle of IMA sensor

The presence of the target leads to the aggregation of IMBs and thus the color change of the solution under the influence of an external magnetic. In this IMA sensor, the dispersed IMBs can selectively capture the target to form the IMB-target complex. We characterized the aggregation of IMBs using dynamic light scattering (DLS). The average diameter of IMBs is 674.4 nm after immuno-reaction before the application of magnetic field, which is larger than that of initial IMBs (207.0 nm) (Figure S1), suggesting the formation of IMB-target complex. We observed the IMBs after immuno-reaction in the magnetic field from different views (front view, side view and top view) at different time intervals (0 s, 5 s and 30 s) (Figure 1). Observing from the front view, the IMBs in both positive and negative samples were initially dispersed. After 5 s, the IMBs in positive sample were partially aggregated and those in negative samples were still dispersed. Until 30 s, all the IMBs were aggregated to a strip and showed a brown color in the positive sample, while the IMBs in the negative sample were still dispersed and the color remained light yellow (Figure 1b and 1c). From the side view and top view, the IMBs in both positive and negative sample can attach to the wall of the tube after 30 s due to the external magnetic field. A remarkable difference between the positive and negative sample is that the aggregated IMBs in the positive sample formed a “dot”,

while IMBs in the negative sample homogenously attached to the wall of the tube and formed an "arc" (Figure 1f to 1g).

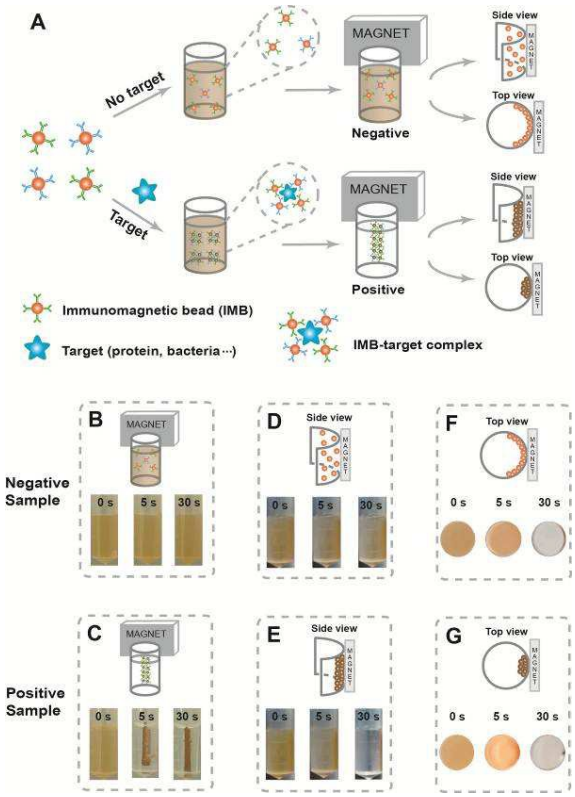

Fig. 1. The schematic diagram of IMA sensor and the change of state of IMBs in the magnetic field viewed from different angles (a) shows that the dispersed IMBs can selectively capture and enrich targets from a sample, and form aggregated IMB-target complex. We use two different monoclonal antibodies to prepare different IMBs for detection of protein. The molar ratio of two antibodies is 1:1. The degree of aggregation of IMBs and the color change of IMBs in the magnetic field can be used as the visual signals in this IMA sensor. (b) to (g) show the state change of IMBs in the magnetic field from different views for detection of *E.coli*. (b) and (c) are front view; (d) and (e) are side view; (f) and (g) are top view. The upper graphs of (b) to (g) show the schematic illustration, and the lower graphs of (b) to (g) show the corresponding experimental results.

We further explored the mechanism of this IMA sensor based on a mechanical analysis of the top view (Figure 2). In this IMA sensor, the force exerted by the magnetic field (F_M) plays a decisive role. The balanced position of IMBs lies in the place where the component force of F_M (F_M cos α) is equal to the maximum of the static friction force (F_{fmax}, which is dependent on the roughness of surface of the reaction tube, and keeps a constant in the same reaction tube). α stands for the angle contained by F_M and F_{fmax}, namely the degree of aggregation of the IMBs. A larger α represents a narrow brown strip, while a smaller α represents a diffuse, yellow coating. In this IMA sensor, F_M ($F_M = 1/6\pi D^3_{IMB}$ B H_d) is related to the diameter of the IMBs (D_{IMB}) and the intensity of the magnetic field (H_d). H_d is distance-dependent and shows the largest intensity when the distance between the magnet and the reaction tube is 0 cm (Figure S2), thus we employ the 0 cm distance (H_0) in our study, and H_0 is kept unchanged in all the other experiments. In such a case, F_M is only related to the diameter of the IMBs (D_{IMB}) and has a third-power relationship with D_{IMB}. Therefore, at the balanced position (F_M cos $\alpha = 1/6\pi D^3_{IMB}$ B H_0), α is merely proportional to the D^3_{IMB}. For positive samples, the immuno-reaction results in the aggregation of IMBs and the D_{IMB} becomes larger than that of negative samples. Consequently, α is much larger in positive samples than that in negative samples at the balanced position, resulting in a narrow brown strip in positive samples while a diffuse, yellow coating in negative samples (Figure 3).

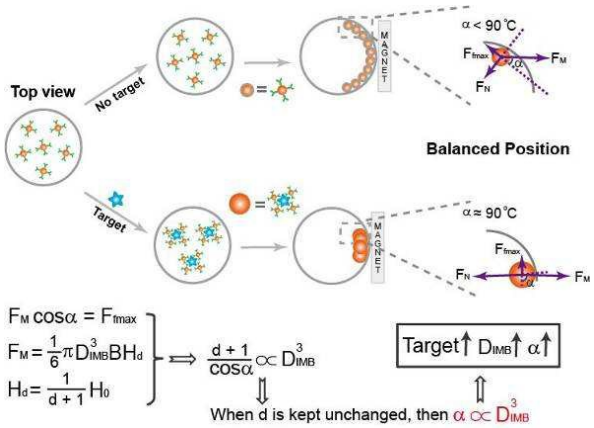

Fig. 2. The mechanical analysis of IMAs from the top view. "F_M" represents the force exerted by the magnetic field; "F_{fmax}" represents the static friction force; "D_{IMB}" represents the size of IMBs; "B" represents the saturation magnetization of IMBs; "H" represents the intensity of added magnetic field (0.05T), "d" represents the distance between the magnet and the tube; H_0 represents the intensity of added magnetic field when the distance of the magnet and the tube is 0 cm.

We further studied the reason why the aggregated IMBs result in the color change of the solution. We found that the color of IMBs solution relates to the concentration of IMBs, since the color of IMBs changes from light yellow into dark brown when the concentration of IMBs is from 0.005 mg/mL to 5 mg/mL (Figure S3). In this IMA sensor, appearance of a brown stripe indicates a positive readout because the aggregated IMBs increase the local concentration of IMBs due to the antibody-antigen interaction, while a diffuse, yellow coating indicates a negative readout because the local concentration of IMBs remain unchanged. Due to the different brightness in color, we can apply the gray value of the IMBs images for the semi-quantitative detection. The gray value is between 180 and 190 when the color of IMBs is yellow, indicating a negative readout. By contrast, the gray value of IMBs is between 190 and 240 when the color of IMBs is brown, which suggests a positive readout (Figure 4 a, 4 c and 4e).

To further validate the principle of this IMA sensor, we also modulate the surface of the reaction tube (rough inside and smooth inside) to vary the static friction force (F_{fmax}). F_{fmax} on the rough tube is larger than that of smooth tube. For the same positive sample, F_{fmax} on the smooth tube leads to a

larger α and thus more heavily aggregated IMBs with a narrow brown strip (Figure S4). By contrast, IMBs in the rough tube is less heavily aggregated due to a larger F_{fmax}. This friction experiment not only further prove the principle of the IMA sensor but also suggests that the degree of aggregation of IMBs relates to the roughness of the reaction tubes, and the smooth tube with a smaller F_{fmax} allows a better performance of this IMA sensor.

Optimization of IMA sensor

We optimize the parameters including the size of IMBs, detection time, the concentration of IMBs and the density of Ab molecules on the surface of IMBs to improve the analytical performance of the IMA sensor. We chose four sizes of MBs (1000 nm, 500 nm, 200 nm and 130 nm) to optimize the performance of the IMA sensor. When 1000 nm and 500 nm MBs are used, we can identify the color difference between the 10^5 cfu/mL *E. coli* and the blank control, and this value is 10^4 cfu/mL for 200 nm and 130 nm MBs (Figure S5).Taken the sensitivity into consideration, 200 nm and 130 nm are more suitable for this IMA sensor. Meanwhile, we found that the suspension stability of 200 nm IMBs is better than that of 1000 nm, 500 nm, 200 nm and 130 nm IMBs. The narrow brown strip with a large section at the top is missing when 1000 nm, 500 nm, and 130 nm are used (Figure S5 a, b, d), and this half-stripe phenomenon will affect the accuracy of the assay, suggesting that the 200 nm IMBs is more suitable in this IMA sensor.

We also investigate the detection time of the IMA sensor to obtain the better performance. Within 30 s, the 1000 nm, 500 nm and 200 nm IMBs are aggregated, while the 130 nm IMBs are still dispersed in the same magnetic fields (Figure S6). When the time is prolonged to 5 min, the degree of aggregation of 130 nm IMBs is higher than that at 30 s, while the degree of aggregation of 1000 nm, 500 nm and 200 nm do not change too much. When the time reaches 20 min, the degree of aggregation of 130 nm IMBs becomes much larger than that at 5 min. The detection time of IMA sensor is 30 s using 1000 nm, 500 nm and 200 nm IMBs, while it takes 20 min using 130 nm IMBs. We presume that this difference is caused by the different saturation magnetization of the IMBs: the saturation magnetization of 130 nm IMBs is smaller than that of 200 nm, 500 nm and 1000 nm IMBs, thus 130 nm IMBs need more time to aggregate into large particles to be separated by the same magnetic field. The sensor using 200 nm IMBs has better sensitivity (10^4 cfu/mL) and response time (30 s) than IMBs of other sizes, so we used 200 nm IMBs for the following experiments.

We further studied the concentration of IMBs and the density of antibody molecules on the surface of IMBs. We found that the sensitivity and accuracy is better when the concentration of IMBs is 75 μg/mL (5×10^8 nanoparticles /mL) (Figure S7b). When the concentration of IMBs is 50 μg/mL, the degree of aggregation of IMBs is not obvious under the condition of 10^4 cfu/mL of *E. coli* (Figure S7c). We found that when the concentration of IMBs is 100 μg/mL, it has a similar sensitivity with that of 75 μg/mL (Figure S7a). Thus, we choose a concentration of 75 μg/mL in this study. For the detection time, we found that the number of magnetic beads does not affect it. We also prepared the IMBs conjugate using different amount of antibodies (0.01mg, 0.1mg and 0.5 mg) and studied the influence of number of antibody (Ab) immobilized on beads on detection efficiency (Figure S8). We found that the sensitivity of this sensor is the best when we use the amount of 0.1 mg Ab (Figure S8b). When a lower amount of Ab (0.01mg Ab) is used, the detection time should be 30 min, because it needs more time to capture and enrich the low concentration of target when little Ab molecules are on the surface of magnetic beads. On the other hand, when lots of Ab molecules are conjugate on the IMBs, the sensitivity of this sensor is affected as well (Figure S8c), because it inhibits the aggregation of the modified IMBs. Therefore, a suitable amount of Ab molecules on the surface of magnetic beads is beneficial to capture the target and form the aggregates of IMBs in this sensor, and we selected this amount of Ab to prepare the IMBs in following experiments.

Sensitivity and Specificity of IMA sensor

To verify the applicability of the IMA sensor, we choose E. coli, alpha fetoprotein (AFP) and carcino-embryonic antigen (CEA) to demonstrate the sensitivity of the approach. The amount of *E.coli* is an important index to evaluate the quality of drinking water, and the cut off value of *E.coli* is 3 cfu/mL in drinking water. AFP and CEA are two important cancer biomarkers that have been widely used as targets in the fields of clinical diagnosis. The cut off value of AFP is 25 ng/mL in human serum and the cut off value of CEA is 5 ng/mL.

GLFS is a popular and simple method for naked-eye detection, we first compare our IMA sensor with GLFS. Figure 3a shows that the color change and the degree of aggregation of IMBs (200 nm) can be identified when the concentration of *E.coli* is between 10^7 cfu/mL and 10^4 cfu/mL. The lowest detectable concentration of the sensor with the naked eye decreases by one order of magnitude compared to GLFS, which shows that IMA sensor has a good sensitivity for the detection of *E.coli* (Figure 3 b). For CEA detection, the color change of IMBs can be distinguished from that of the blank sample when the concentration of CEA is 2 ng/mL, a 10-fold increase in sensitivity compared with GLFS (Figure 3c and 3d). The degree of aggregation of IMBs relates to the concentration of CEA (from 20 ng/mL to 2 ng/mL). The IMBs show a narrow line when the concentration of CEA is 20 ng/mL, and the IMBs show a wide line when the concentration of CEA is 2 ng/mL. Thus, the degree of aggregation of IMBs can be used as another signal readout. For AFP detection, the color change of IMBs can be distinguished by naked eyes when the concentration of AFP is 3 ng/mL, which is about 7-fold increase in sensitivity (Figure 3e and 3f). The result shows that the sensitivity of IMA sensor is better than that of GLFS, and its analysis time (15 min) and simplicity (one step) are as good as that of GLFS. Therefore, IMA sensor has great potential in point-of-care testing.

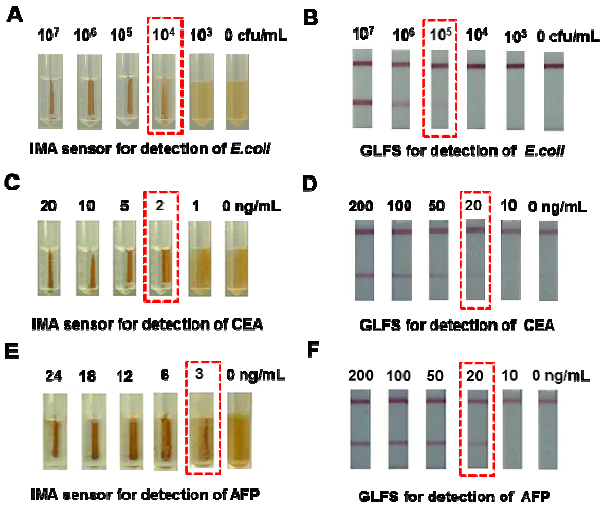

Fig. 3. The IMA sensors and GLFS for the naked-eye detections of *E.coli*, CEA and AFP. In (a) and (b), the concentration of *E.coli* is 0, 10^3, 10^4, 10^5, 10^6, and 10^7 cfu/mL. In (c), the concentration of CEA is 0, 1, 2, 5, 10, and 20 ng/mL; in (d), the concentration of CEA is 0, 3, 6, 12, 25, 50, 100, and 200 ng/mL; In (e), the concentration of AFP is 0, 3, 6, 12, 18, and 24 ng/mL; in (f), the concentration of AFP is 0, 4.5, 9, 18, 36, 75 and 150 ng/mL. The size of IMBs is 200 nm, the concentration of IMBs is 75μg/mL, and the volume of the tube is 2 mL. The red dotted line shows the lowest detectable concentration in each sample.

ELISA is another widely used method in diagnosis field due to its relatively high sensitivity, quantification and high throughput. We also compare the sensitivity and the operation of this IMA sensor with ELISA. We apply the gray value of the IMBs images for semi-quantitative detection of the targets. For comparison, we compare the results of ELISA with the gray-scale value results of IMA sensor. The limit of detection (LOD, three times the standard deviation) of ELISA for detection of *E.coli* is 10^4 cfu/mL, the same level as the IMA sensor (Figure 4a and Figure 4b). The LOD of ELISA for detection of CEA and AFP is 3.4 ng/mL and 4.2 ng/mL, respectively (Figure 4d and Figure 4f). The LOD of this IMA sensor for detection of CEA and AFP is 1.5 ng/mL and 3.3 ng/mL (Figure 4 c and Figure 4e), indicating that the sensitivity of IMA sensor for cancer biomarkers detection is better than that of ELISA and GLFS. Therefore, this IMA sensor allows the same level of sensitivity as ELISA without complex protocols. Meanwhile, it can realize one-step detection within 15min, which can avoid multi-washing steps that is needed in ELISA.

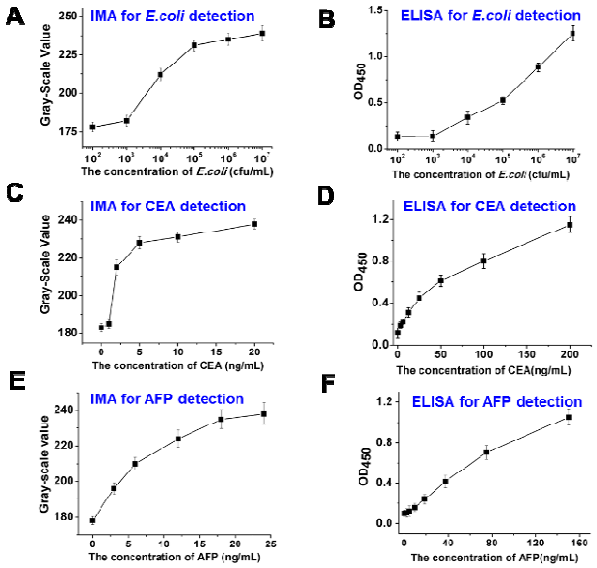

Fig. 4. IMA sensor and ELISA for detections of *E.coli*, CEA and AFP. In (a) and (b), the concentration of *E.coli* is 0, 10^2, 10^3, 10^4, 10^5, 10^6, and 10^7 cfu/mL. In (c), the concentration of CEA is 0, 1, 2, 5, 10, and 20ng/mL; in (d), the concentration of CEA is 0, 3, 6, 12, 25, 50, 100, and 200 ng/mL. In (e), the concentration of AFP is 0, 3, 6, 12, 18, and 24 ng/mL; in (f), the concentration of AFP is 0, 4.5, 9, 18, 36, 75 and 150 ng/mL. The error bars represent the standard deviation of three measurements.

We also investigate the selectivity of the IMA sensor. During the analysis of *E.coli*, the other four bacteria, *Salmonella spp* (*S.spp*), *Shigella spp*, *Staphylococcus aureus* (*S. aureus*) and *Spirillum Cholera* (*S. cholera*) are used to evaluate the specificity of the IMA sensor. The degree of aggregation and the color change of IMBs are remarkable in *E.coli*, and the other bacterial samples show little aggregation (Figure 5), which confirms that the sensor has good specificity for *E.coli* detection. To confirm that the selectivity of this sensor is dependent on the specific recognition between antibody and antigen, and it is not affected by the concentration of bacteria. We also chose the 10^6 cfu/mL of *E.coli* to carry out the selectivity experiment, and the result further shows that this IMA sensor has good selectivity for detection of *E.coli* (Figure S9).

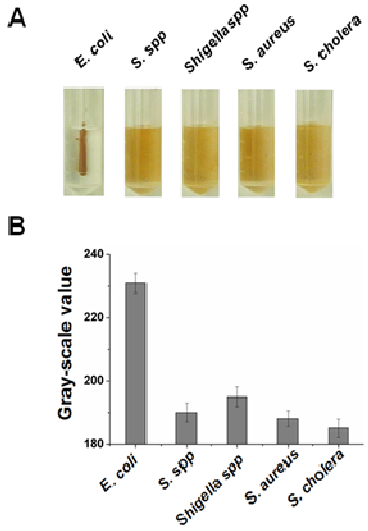

Fig. 5. The selectivity of IMA sensor for detection of *E.coli*. Five bacteria (*E. coli*, *Salmonella spp*, *Shigella spp*, *Staphylococcus aureus* and *spirillum cholera*) were selected to evaluate the specificity of IMA sensor. The concentration of these bacteria was 10^5 cfu/mL.

Robustness of IMA sensor

Besides the sensitivity and selectivity, robustness and cost are also very important factors to evaluate a sensor, which largely determine its practical application. The IMBs are very stable and can be kept well between 4-8°C for six months, without compromising the assaying performance compared to freshly prepared IMBs (Figure S10). Previous works have reported that coverage of antibody on the surface of magnetic beads is controllable and repeatable, and that 1 μm magnetic beads can conjugate 10^4 to 10^5 protein molecules which can be used as carriers for signal amplification.[23] Meanwhile, the IMBs (either aggregated or dispersed) are stable after 24 h in the magnetic field without affecting the results of the IMA sensor (Figure S11). We also successfully carried out the detection of *E. coli* in either 2 mL tubes or 1.5 mL tubes (Figure S12), which indicates that the IMA sensor is very robust. Other factors including salt concentration, pH and foreign proteins that exist in real biological fluids show little interference on this IMA sensor, as shown in the real sample analysis.

Real sample analysis

The IMA sensor can be applied to analyze real samples, including detection of *E. coli* in water samples from diverse sources, and CEA/AFP in spiked urine samples and real serum samples.

We first apply IMA sensor to detect *E.coli* in river water samples. Six river water samples were from different locations in the same river. The concentrations of spiked *E.coli* in sample 1, sample 2 and sample 3 were 10^4, 10^5 and 10^6 cfu/mL, and sample 4 to sample 6 were not spiked with *E.coli*. Figure 6a shows that the IMBs in sample 1, 2 and 3 are heavily aggregated, and IMBs in other samples are well dispersed, suggesting that the sensor can successfully detect *E.coli* in river water samples. To further verify the potential application of IMA sensor for detection of *E.coli*, we choose the water samples from a livestock farm, where it is often contaminated by *E.coli*. Sample 1 to sample 6 were not spiked with *E.coli*. Sample 6 is detected to be a positive sample and other samples are free of *E.coli* (Figure 6e, samples 1-5). The results agree well with the results of ELISA (Figure 6c and Figure 6f), indicating that the IMA sensor can precisely detect *E.coli* in real samples.

For cancer biomarkers analysis, we employed this sensor for detection of CEA and AFP in spiked urine samples and clinical serum samples. The urine samples were from healthy people in our lab, and clinical serum samples were from a local hospital. When AFP and CEA are spiked in urine samples, the lowest detectable concentration of IMA sensor with the naked eye for detection of AFP and CEA are 2.5 ng/mL and 2 ng/mL, respectively (Figure S13). This IMA sensor also can detect CEA and AFP in clinical serum samples. For CEA detection, sample 1 to 3 and sample 5 were detected to be positive samples, and sample 4 and sample 6 were detected to be negative samples (Figure 7a and 7c). For AFP detection, sample 1, sample 2, sample 4 and sample 5 were detected to be positive samples, and sample 3 and sample 6 were detected to be negative samples (Figure 7b and 7d). The results of this IMA sensor for detection of cancer biomarkers agree well with that of ELISA (Figure 7c and 7f), which indicates that this IMA sensor can be used for detection of cancer biomarkers in real clinical samples.

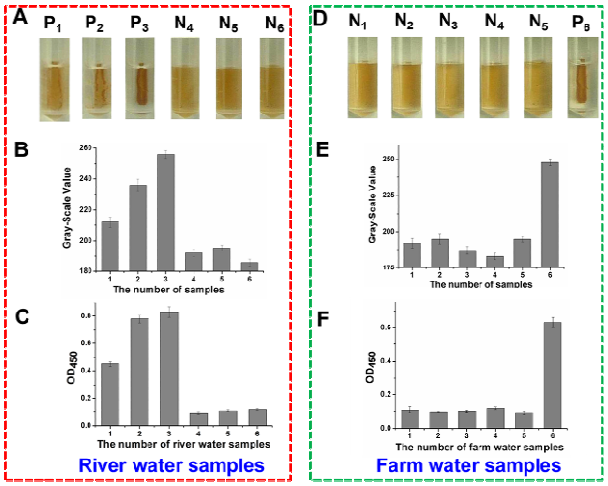

Fig. 6. The IMA sensor and ELISA for detection of *E.coli* in water samples from different sources. (a), (b) and (c) respectively show the result that the IMA sensor and ELISA for the analysis of spiked river water samples. *E.coli* in sample P1, sample P2 and sample P3 was spiked with 10^4, 10^5 and 10^6 cfu/mL, respectively, and the other samples which were from different locations in the same river were not spiked with *E.coli*. (d), (e) and (f) show the result that the IMA sensor and ELISA, respectively. Six water samples were from livestock farm and not spiked with *E.coli*.

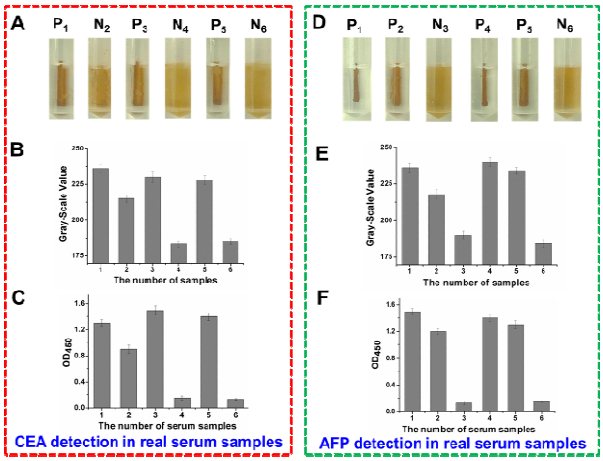

Fig. 7. The IMA sensor and ELISA for detection of AFP and CEA in real clinical samples. The real serum samples were diluted by 100 folds using PBS solution. (a) and (d) show the visual results of the IMA sensor for detection of CEA and AFP; (b) and (e) show the quantitative results for detection of CEA and AFP by using the gray-scale value to quantify the color change of IMBs; (c) and (f) show the results of ELISA for detection of CEA and AFP in serum samples.

Therefore, we can apply the IMA sensor to carry out microbial assay in many kinds of water samples, and cancer biomarkers in real clinical serum samples. Compared to conventional ELISA and GLFS, this sensor has many advantages: (1) speediness and simplicity: the sensor combines the magnetic capture and detection into one step, thus can reduce the whole analysis time (10-15min), which is more rapid and friendly operable than that of ELISA. It only needs a magnetic separation rack, and does not need professional operators; (2) sensitivity: the LOD of this sensor for determination of *E.coli* decreases by one order of magnitude compared with GLFS, which compares to that of ELISA. Therefore, the IMA sensor will be a reliable and potential strategy for POC testing. However, a potential limitation is that the linear detection range of IMA sensor is narrow (10^3-10^5 cfu/mL for detection of *E.coli* in IMA sensor). The comparison of ELISA, GLFS and IMA sensor for detection of *E. coli* is shown in Table 1.

Table.1 The comparison of ELISA, GLFS and IMA sensor for detection of *E. coli*

	Sensitivity	Detection time	Application
ELISA	10^4 cfu/mL	2-4 h	Quantitative analysis
GLFS	10^5 cfu/mL	10 min	Semi-quantitative analysis
IMA sensor	10^4 cfu/mL	15 min	Semi-quantitative analysis

Conclusions

We developed an immunosensor based on the aggregation of IMBs for one-step detection of pathogens and cancer biomarkers in real samples. IMBs act as the optical readout for assays in this approach, in addition to serving as the carrier for purification/separation. The target analytes result in the aggregation of initially dispersed IMBs that can be identified by the naked eyes according to the color change of IMBs. The LOD of this sensor decreases by one order of magnitude compared with GLFS, and the detection time is as fast as GLFS. This IMA sensor combines the magnetic capture and visual detection into one step, which can simplify the whole detection process. It is highly promising that this IMA sensor can be easily developed into a rapid, sensitive and low-cost diagnostic tool to meet the needs of POC testing, particularly with low-resource settings in developing countries.

Acknowledgement

We thank the National Natural Science Foundation of China (81361140345, 21505027, 51373043, 21535001), the Chinese Academy of Sciences (XDA09030305), the Ministry of Health (2012ZX10001-008), and the CAS/SAFEA International Partnership Program for Creative Research Teams and Wang Bao-en Liver Fibrosis Foundation (2011029) for financial support.

Notes and references

1. J. Sun, Y. Xianyu and X. Jiang, *Chem. Soc. Rev.*, 2014, **43**, 6239-6253.
2. L. Yan, Z. Zhu, Y. Zou, Y. Huang, D. Liu, S. Jia, D. Xu, M. Wu, Y. Zhou, S. Zhou and C. J. Yang, *J. Am. Chem. Soc.*, 2013, **135**, 3748-3751.
3. Y. Zhang, L. Zhang, J. Sun, Y. Liu, X. Ma, S. Cui, L. Ma, J. J. Xi and X. Jiang, *Anal. Chem.*, 2014, **86**, 7057-7062.
4. X. Mao, Y. Ma, A. Zhang, L. Zhang, L. Zeng and G. Liu, *Anal. Chem.*, 2009, **81**, 1660-1668.
5. N. Thaitrong, R. Charlermroj, O. Himananto, C. Seepiban and N. Karoonuthaisiri, *Plos One*, 2013, **8**, e8323.
6. H. Wang, G. Li, Y. Wu, F. Yuan and Y. Chen, *Food Chem.*, 2014, **147**, 106-110.
7. J. Chen, Z. Fang, P. Lie and L. Zeng, *Anal. Chem.*, 2012, **84**, 6321-6325.
8. Y. Xiang and Y. Lu, *Nat. Chem.*, 2011, **3**, 697-703.
9. D. Liu, W. Chen, Y. Tian, S. He, W. Zheng, J. Sun, Z. Wang and X. Jiang, *Adv. Healthc. Mater.*, 2012, **1**, 90-95.
10. R. de la Rica and M. M. Stevens, *Nat. Nanotechnol.*, 2012, **7**, 821-824.
11. S. Sharma, J. Zapatero-Rodriguez, P. Estrela and R. O'Kennedy, *Biosensors*, 2015, **5**, 577-601.
12. V. Gubala, L. F. Harris, A. J. Ricco, M. X. Tan and D. E. Williams, *Anal. Chem.*, 2012, **84**, 487-515.
13. J. H. Soh, Y. Lin, S. Rana, J. Y. Ying and M. M. Stevens, *Anal. Chem.*, 2015, **87**, 7644-7652.
14. S. Gupta, H. Andresen, J. E. Ghadiali and M. M. Stevens, *Small*, 2010, **6**, 1509-1513.
15. H. Andresen, M. Mager, M. Griessner, P. Charchar, N. Todorova, N. Bell, G. Theocharidis, S. Bertazzo, I. Yarovsky and M. M. Stevens, *Chem. Mater.*, 2014, **26**, 4696-4704.
16. R. Malhotra, V. Patel, B. V. Chikkaveeraiah, B. S. Munge, S. C. Cheong, R. B. Zain, M. T. Abraham, D. K. Dey, J. S. Gutkind and J. F. Rusling, *Anal. Chem.*, 2012, **84**, 6249-6255.
17. H. J. Chung, C. M. Castro, H. Im, H. Lee and R. Weissleder, *Nat. Nanotechnol.*, 2013, **8**, 369-375.

18. B. S. Munge, A. L. Coffey, J. M. Doucette, B. K. Somba, R. Malhotra, V. Patel, J. S. Gutkind and J. F. Rusling, *Angew. Chem. Int. Edit.*, 2011, **50**, 7915-7918.
19. C. S. Jeon, I. Hwang and T. D. Chung, Adv. *Funct. Mater.*, 2013, **23**, 1484-1489.
20. H. C. Tekin and M. A. M. Gijs, *Lab Chip*, 2013, **13**, 4711-4739.
21.L. Tang, J. Casas and M. Venkataramasubramani, *Anal. Chem.*, 2013, **85**, 1431-1439.
22. D. C. Leslie, J. Li, B. C. Strachan, M. R. Begley, D. Finkler, L. A. L. Bazydlo, N. S. Barker, D. M. Haverstick, M. Utz and J. P. Landers, *J. Am. Chem. Soc.*, 2012, **134**, 5689-5696.
23. V. Mani, D. P. Wasalathanthri, A. A. Joshi, C. V. Kumar and J. F. Rusling, *Anal. Chem*., 2012, **84**, 10485-10491.